Observation of Clump Structure in Transported Particle Orbit Using an Upgraded Neutral Particle Analyzer during TAE Burst in LHD

S. Kamio[1], Y. Fujiwara[1], K. Nagaoka[1,2], K. Ogawa[1,3], R. Seki[1,3], H. Yamaguchi[1], H. Nuga[1], M. Isobe[1,3], M. Osakabe[1,3], C. Z. Cheng[4,5], and the LHD Experiment Group[1]

[1]National Institute for Fusion Science, National Institutes of Natural Sciences, Toki, Gifu 509-5292, Japan.

[2]Graduate School of Science, Nagoya University, Nagoya, Aichi 464-8603, Japan.

[3]The Graduate University for Advanced Studies, SOKENDAI, Toki, Gifu 509-5292, Japan.

[4]Graduate School of Frontier Sciences, The University of Tokyo, Kashiwa, Chiba 113-0033, Japan.

[5]Princeton Plasma Physics Laboratory, Princeton University, Princeton, NJ 08543, USA.

kamio@nifs.ac.jp

Abstract

TAE bursts are often observed in relatively low magnetic field experiments in LHD with tangential NB injection. During TAE bursts, hole-clump pairs in real space were observed in previous studies. In order to observe the behavior of the energetic particles during TAE bursts in more detail, a tangential E-parallel-B type neutral particle analyzer (E||B-NPA) was upgraded to improve the time resolution up to 100 kilo samples per second by updating its measurement electronic circuits. Using this high time resolution E||B-NPA, the clump formations are clearly observed in real space. In order

to analyze the observed particles with high time resolution, conditional averaging technique is used. The lost energetic particles with 150 keV were initially observed just before the TAE burst, and the energy decreases faster than the classical slowing down time. The energetic particles transported by the TAE burst were detected with energy slowing down time of 6-8 ms for more than 6 ms after the TAE burst finished. According to the orbit trace code LORBIT calculation, the particle pitch angle and the radial location ($\rho = r/a_{99}$) of the energetic particles resonating with the TAE mode frequency are increased by 5 degrees and 0.2, respectively, during TAE bursts. These results are consistent with the observed downward frequency chirping of the magnetic fluctuation. By comparing the energy of the detected particles by E||B-NPA and the corresponding frequency of the magnetic fluctuation, the pitch angles of the resonant particles are considered to be 15-25 degrees at 150 keV before they are transported by the TAE burst. The frequency chirping of the magnetic fluctuation shows good agreement with the observed clump structure by considering the pitch angle of the resonant particles.

1. Introduction

Toroidal Alfvèn eigenmodes (TAEs) [1] are being studied numerically [2,3] and experimentally [4-6] because of their practical importance for the future fusion reactor. In burning plasmas, energetic particles generated by fusion or by external heating can drive the TAE unstable. The TAE deteriorates fast-ion confinement which adversely affects heating and may cause damage to the first wall. The spontaneous formation of “clump and hole” phase-space structures have been shown in

kinetic simulation studies [7,8], and TAE frequency sweeping is often observed in many devices [9-12]. The particle transport due to the TAE has also been investigated in the Large Helical Device (LHD) [13]. Magnetic fluctuations of the TAE bursts are observed in relatively low magnetic field (0.6 T at the magnetic axis) experiments. The ratio of the typical beam velocity and the Alfvèn velocity is approximately v_b/v_A=1.5. Therefore, TAE activities can be observed with the TAE resonance condition of $v_{||}=v_A$ by considering the pitch angle and/or the energy slowing down of the beam ions in this experimental condition.

By measuring the charge exchanged neutral particles using E-parallel-B type neutral particle analyzer (E||B-NPA) [14] and by measuring the lost ion using scintillator-based fast-ion loss detector (FILD) [15-17], the existence of the hole-clump pairs was suggested in real space. From the slowing down time analysis, the location of each lost particle orbit was identified. Simultaneous observation of hole-clump formations reveals the enhanced radial transport of energetic particles in plasma by TAE bursts.

In this paper, we report the results of the TAE burst experiments using upgraded E||B-NPA with improved time resolution. The energy distributions of the energetic neutrals are clearly observed together with the magnetic fluctuations. Assuming the resonance condition of $v_{||}=v_A$, the frequency chirping of the magnetic fluctuations are fitted with the energy slowing down of the energetic neutrals by adjusting the pitch angle θ of the resonance particles.

2. Experimental setup

Figure 1 shows the schematic view of the LHD with the typical plasma flux surfaces (red and pink lines) and the tangential line of sight of the E||B-NPA (blue line). The line of sight of the E||B-NPA is 50-85 mm below the mid-plane. The E||B-NPA measures the energetic particles injected by neutral beam injectors (NBIs) #1 and #3. These tangentially injecting NBIs are based on the negative-ion sources and can inject with energy of up to 180 keV. The location of the E||B-NPA is fixed and the line of sight cannot be altered. The energy range of the E||B-NPA can be changed by changing the magnetic field and the electric field inside the E||B-NPA vacuum chamber [18]. In order to upgrade the time resolution, new electronics were installed [19]. The upgrades shortened the pulse width of a single particle from 125 ns to 5 ns and the sampling time was improved from 250 μs to 10 μs. The measurement ρ and the pitch angle θ along the line of sight of the E||B-NPA are shown in Fig.2. Because the NPA measures the energetic particles which exchanged charge with neutral particles, the measuring region is considered to be the outside region where the neutral density is high. At around the ρ=1 of near side to the E||B-NPA, the θ is 23 degrees for the TAE burst experiments with R_{ax}=3.8 m. It is noted that R_{ax} is major radius of the magnetic axis shifted from the vacuum condition of R_{ax0}=3.6 m.

Toroidal and poloidal mode numbers are determined using 6 toroidal and 15 poloidal Mirnov coils with a sampling rate of 1 MHz. The spatial distributions of the electron temperature and the electron density are measured by Thomson scattering.

3. Results and discussions

In order to measure the energetic particles transported by TAE bursts using the upgraded E||B-NPA, NBI #1 is used as the energetic ion source. The magnetic field at the magnetic axis is 0.6 T and the major radius is 3.8 m. Because of the low magnetic field, electron cyclotron resonance heating (ECRH) cannot be used for the plasma startup. Instead of the ECRH, the initial plasma is generated by using NBIs [20]. Typical waveforms of TAE burst experiments are shown in Fig.3 (a)-(f). The timing of 4.4-4.85 seconds sustained by the single co-NBI are used for the investigation of the TAE bursts. During the period, there was no significant change in the plasma stored energy shown in Fig.3 (c), electron density and electron temperature shown in Fig.3 (e). The plasma current Fig.3 (d) gradually increased by the neutral beam current drive (NBCD) during the constant injection of co-NBI. Fig.3 (f) is the signal of Mirnov coil with high-pass processing at 30 kHz. MHD instabilities were observed during the timing of co-NBI injection. Figure 4 (a)-(d) focused on the timing of the TAE bursts clearly observed by E||B-NPA. The peak amplitude of the observed magnetic fluctuations shown in Fig.4 (a) is 2-3x10^{-5} T, and the spectrogram shown in Fig.4 (b) were calculated

with a FFT window of 200 μs. Figure 4 (c) is the time evolution of the energy spectrum of particle flux Γ observed by E||B-NPA. The energetic particles which are transported by the TAE burst are clearly observed and the energy is decreasing after the TAE burst. The spatial distributions of the electron density and the temperature during the TAE burst are shown in Fig. 5. The electron temperature is approximately 0.7-0.8 keV at the magnetic axis, and the electron density is 1.1-1.4x10^{19} m^{-3} with the hollow profile. Figure 6 shows the spectrogram of the magnetic fluctuation amplitude focused on the single TAE burst and the toroidal distribution of the derivative of the magnetic field at Mirnov coil. Before the large fluctuation at t~4.5009 s, a small fluctuation with similar frequency was observed at t~4.5004 s. The toroidal mode number n was 1, and the poloidal mode number m was a mix of 1 and 2. Figure 7 shows the shear Alfvèn spectrum calculated by the STELLGAP code [21], which is developed for three-dimensional configurations. The plasma parameters of at the 4.5 s of #152781 and the magnetic field distribution of the vacuum conditions are used for the calculation. The TAE gap of n=1 and m=1+2 mode appeared at around ρ=0.4-0.5 with the frequency of approximately 50 kHz. This frequency is similar to the experimentally observed 50-80 kHz which is shown in Fig. 6.

Figure 8 (a) shows the dependence of the fluctuation amplitude of the “burst to burst” interval. The intervals were 5-20 ms. A longer interval induces a larger burst. In the case of a TAE burst with a short interval, the transported and lost ions are not fully replenished. The fast-ion pressure is considered to affect the amount of resonant particles in a TAE burst. The relationship between the

amplitude of the fluctuation and the amount of the increasing flux due to the TAE burst ΔΓ during the TAE burst is shown in Fig. 8 (b). Figure 9 shows the time evolution of the amplitude of the magnetic fluctuation, and the ΔΓ measured by E||B-NPA. Because the TAE bursts are observed at 4.4-4.85 seconds as shown in Fig. 4 (d), the Γ without TAE burst is measured before 4.4 s and after 4.85 s. The peak of the average counting rate of ΔΓ is approximately 5-10 counts per 10 μs. Therefore, it is difficult to investigate with high time resolution. In order to investigate the detailed shape with high time resolution, conditional averaging technique is used to counteract the low count rate. 72 TAE bursts across two similar discharges were averaged. To align the timing of each burst, the peak amplitude of the magnetic fluctuation of 70 kHz is set to 2.0 ms. By averaging 72 bursts, the clump shape can be seen clearly even with the time resolution of 10 μs. The vertical red dashed lines are the timing of the start and the timing of the end of the TAE bursts. The clump has different behavior between during the TAE burst and after the TAE burst. During the TAE burst, the energy of the ΔΓ decrease with the slowing down time of 1.0-1.5 ms. This short slowing down time is difficult to consider as the classical energy slowing down time. This energy slowing down is considered to be related to the frequency chirping. After the TAE burst, the energy slowing down time is 6-8 ms, and the ΔΓ is gradually decreased. However, the clump is still remaining more than 6 ms after the end of the magnetic fluctuation of the TAE burst. The yellow line in the Fig. 9 indicates the injection energy of the NBI #1. The NBI injection energy is higher than the highest energy of the observed ΔΓ at 150 keV. Similar fluctuation chirping can be confirmed at 0.5 ms before the large bursting fluctuation

between the red dashed lines. As the results of the repeated transportation of energetic particles by the TAE bursts, Γ of between the burst and burst is lower than that of without the TAE burst. For this reason, ΔΓ is negative at the region between 50-150 keV without clump. Because some of the intervals of burst to burst are shorter than 8 ms, the previous clump can be seen in 0-2 ms at less than 80 keV and in 8-10 ms at more than 100 keV.

In order to investigate the clump shape in more detail, we divided the conditional averaging into three groups by the amplitude of the magnetic fluctuation at 75-80 kHz. Figure 10 (a) shows the peak amplitude of the magnetic fluctuations of each frequency. The amplitude of the magnetic fluctuations are clearly decreased at more than 70-80 kHz and at less than 50 kHz. The TAE coupling frequency is considered to be 50-80 kHz in this experiment. The large burst group has 14 bursts, the medium burst group has 23 bursts, and the small burst group has 35 bursts. The numbers of the bursts for each group were decided to have the same total ΔΓ. The energy distribution of Γ without TAE burst, and during the TAE burst of three groups are shown in Fig. 10 (b). As with the conditional averaging in Fig. 9, the peak amplitude of the magnetic fluctuation of 70 kHz is set to 2.0 ms. The Γ subsidence between the burst and burst is approximately 0.2-0.4 counts per 10 μs. On the other hand, hole formation can be seen at lower Γ than between the burst and burst, such as at 160 keV of 2.0-2.5 ms and at 150 keV of 3.0-3.5 ms. However, the hole formation is difficult to identify because the ΔΓ of clump has a much higher counting rate than that of hole. The counting rate of the clump is also higher than the Γ. Contrary to the frequency distributions of the amplitude in Fig. 10 (a), the

counting rate energy distributions of three groups are similar at the high energy region and different at the low energy region. Figure 11 shows the time evolutions of the averaged spectrogram of the magnetic fluctuations and the total $\Delta\Gamma$ and its energy slowing down time fitting curves. The energy slowing down times are 7.5-8.1 ms and 6.2-6.4 ms for 150 keV and 100 keV particles, respectively. As shown in Fig. 12, the energy slowing down time of Γ is approximately 9.7 ms obtained at the turning off timing of the NBI #1 of the same discharge. The slowing down time of the $\Delta\Gamma$ after the TAE bursts are shorter than that of Γ before the TAE bursts. These results indicate that the orbit of the transported particles pass through the outer region where τ_s is very low. The energetic particles which are resonant with the TAE bursts are transported to the outer orbit, and remain in the outer orbit until energy decay.

Figure 13 shows the results of the Lorenz orbit cord LORBIT [22] calculated for this experimental condition. Orbit of the energetic particles are tracked with the full gyromotion in the collisionless condition. The distribution of the magnetic field in the vacuum condition are used for the calculation. The orbits are traced from along the line of sight of E||B-NPA. The horizontal axis of the Fig. 13 (a) is the initial location of the orbit trace. We traced the orbit from various ρ_{LOS} on the line of sight, and calculated the slowing down time using the electron temperatures and densities along the orbit. As the result of the initial ρ_{LOS} scan, ρ_{LOS}=1.06-1.09 are considered to be the location of the energetic particles charge exchanging because the slowing down times are similar to the fitting curves in Fig. 11 after the TAE burst. Figure 13 (b) shows the ρ and the θ along the traced orbit with the initial

energy of 150 keV and 100 keV. The color contours indicate the time duration while the particle pass through the ρ with the θ. The yellow circles indicate the initial location of the orbit trace. Although the ρ and θ of the resonance position cannot be identified in the orbits, the duration time is equivalent to the possibility to be the ρ and θ of the resonance position. Therefore, we referred to the higher region to understand the trends. The ρ of the higher region is consistent with the result of the shear Alfvèn spectrum shown in Fig.7. According to the results, the ρ considered to shift to outside approximately 0.2 and θ considered to increase approximately 5 degrees with the resonant particle energy decrease during TAE burst frequency chirping.

With considering the results of the LORBIT, the peak amplitude of the magnetic fluctuations are over plotted with the ΔΓ in Fig. 14 (a). The white asterisks are peak of the magnetic fluctuations with the corresponding energy. The frequencies of the magnetic fluctuations are shown with the energy of the resonant particles with the relation of $v_{\|}=v_{\mathrm{A}}$, written as follows.

$$E_{\mathrm{res}} = \frac{1}{2} m_{\mathrm{i}} v^2 = \frac{1}{2} m_{\mathrm{i}} {v_{\mathrm{A}}}^2 / \cos\theta^2 \ (\text{assuming } v_{\|} = v_{\mathrm{A}}),$$

where

$$v_A = (4\pi R_{\mathrm{ax}} q_{\mathrm{TAE}}) f_{\mathrm{TAE}},$$

$$q_{\mathrm{TAE}} = (m + 1/2)/n = 3/2,$$

and θ is the pitch angle of the resonance particles. The θ of the three cases were chosen to fit the fluctuations to the initial timing of the increase of the ΔΓ in each energy. As the results of the fitting, initial θ at 150 keV are 15, 20, and 25 degrees. Because the θ increases approximately 5 degrees during the frequency chirping from the result of the LORBIT, the θ for the fitting are changed also in the Fig. 14 (a). As the result of the conversion of frequency to energy using these θ, the highest energies of three groups are 180 keV, and the lowest energies are 110, 100, and 90 keV. These results are in good agreement with the energy slowing down of the initial ΔΓ. The energetic particles are not observed at more than 160 keV despite the magnetic fluctuations being observed. However, it can be considered that the orbit of the energetic particle does not pass through the line of sight at $\rho>1$. Actually, the energetic particles at more than 170 keV injected by NBI are not observed by E||B-NPA. Figure 14 (b) shows the relationship between the peak amplitude of the magnetic fluctuation and the total ΔΓ of 0.1 ms after the peak of the fluctuations in each energy. In order to compare the magnitude of the magnetic fluctuation and the resonated energetic particles observed by E||B-NPA, the ΔΓ integration times are shortened to 0.1 ms. The colors of the symbols indicate the energy of the ΔΓ and magnetic fluctuation. The symbols of circle, triangle, and diamond are obtained from large, medium, and small group, respectively. By dividing the resonant particle energies, the relationship between the amplitude of the magnetic fluctuation of the TAE bursts and observed resonance particles by E||B-NPA could be clarified experimentally in the real space and in the phase space.

4. Conclusion

The TAE burst experiments are demonstrated using an upgraded E||B-NPA with the sampling time of 10 μs. By the conditional averaging technique, the clump formation was clearly confirmed during and after the TAE burst. In order to investigate the behavior in more detail, we clarified into three similar bursting groups. The local resonant ρ can be estimated by the slowing down time after the TAE burst and the results of the orbit trace calculation by LORBIT. Furthermore, by considering the increase of the resonant particle pitch angle θ during the frequency chirping, the relationship of the magnetic fluctuation frequency chirping and the energy slowing down of ΔΓ during TAE bursts are well explained. By comparing the amplitude of the magnetic fluctuations and the observed resonance particles by E||B-NPA in each energy, the relationship could be clarified in the real space and in the phase space.

Acknowledgments

This work was supported by NIFS Grant No. ULRR006, ULRR035, and ULRR702.

References

[1] Cheng C. Z. and Chance M. S. 1986 *Phys. Fluids* **29** 3695.

[2] Todo Y., Berk H. L. and Breizman B. N. 2003 *Phys. Plasmas* **10** 2888.

[3] Zhu J., Ma Z. W. and Fu G. Y. 2014 *Nucl. Fusion* **54** 123020.

[4] Heidbrink W. W. et al 1991 *Nucl. Fusion* **31** 1635.

[5] Darrow D. S. *et al* 1997 *Nucl. Fusion* **37** 939.

[6] Isobe M. *et al* 2010 *Fusion Sci. Tech.* **58** 426.

[7] Berk H. L. *et al* 1997 *Phys. Lett. A* **234** 213.

[8] Berk H. L. *et al* 1999 *Phys. Plssmas* **6** 3102.

[9] Heidbrink W. W. 1994 *Plasma Phys. Control. Fusion* **37** 4120.

[10] Shinohara K. *et al* 2001 *Nucl. Fusion* **41** 603.

[11] Pinches S. D. *et al* 2004 *Plasma Phys. Control. Fusion* **46** S47-S57.

[12] Gryaznevich M. P. and Sharapov S. E. 2006 *Nucl. Fusion* **46** S942-S950.

[13] Toi K. *et al* 2004 *Plasma Phys. Control. Fusion* **46** S1.

[14] Osakabe M. *et al* 2006 *Nucl. Fusion* **46** S911-S917.

[15] Ogawa K. *et al* 2008 *Plasma Fusion Res.* **3** S1082.

[16] Ogawa K. *et al* 2009 *J. Plasma Fusion Res. SERIES* **8** 655.

[17] Ogawa K. *et al* 2010 *Nucl. Fusion* **50** 084005.

[18] Medley S. S. and Roquemore A. L. 1998 *Rev. Sci. Instrum.* **69** 2651.

[19] Fujiwara Y. *et al* 2019 *JINST* (to be published).

[20] Kaneko O. *et al* 1999 *Nucl. Fusion* 39 1087.

[21] Spong D. A. *et al* 2010 *Phys Plasmas* **17** 022106.

[22] Isobe M. *et al* 2009 *J. Plasma Fusion Res. SERIES*, **8** 330.

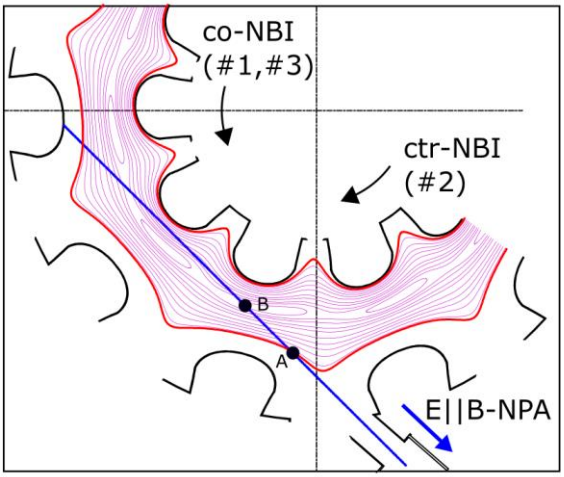

Figure 1. Schematic view of the LHD and the line of sight of the E-parallel-B type neutral particle analyzer (E||B-NPA). E||B-NPA can measure the lost energetic particles injected by NBI #1 and NBI #3. The locations of A and B correspond to A and B in Fig. 2.

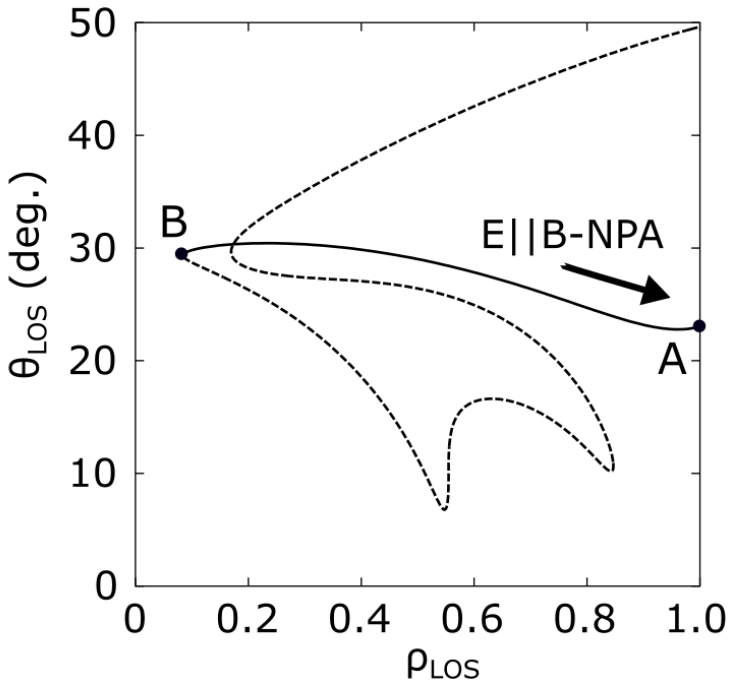

Figure 2. The radial position ρ and the pitch angle θ of lost particles detected along the line of sight of the E||B-NPA. The ρ and θ of A and B correspond to the location of A and B in Fig. 1.

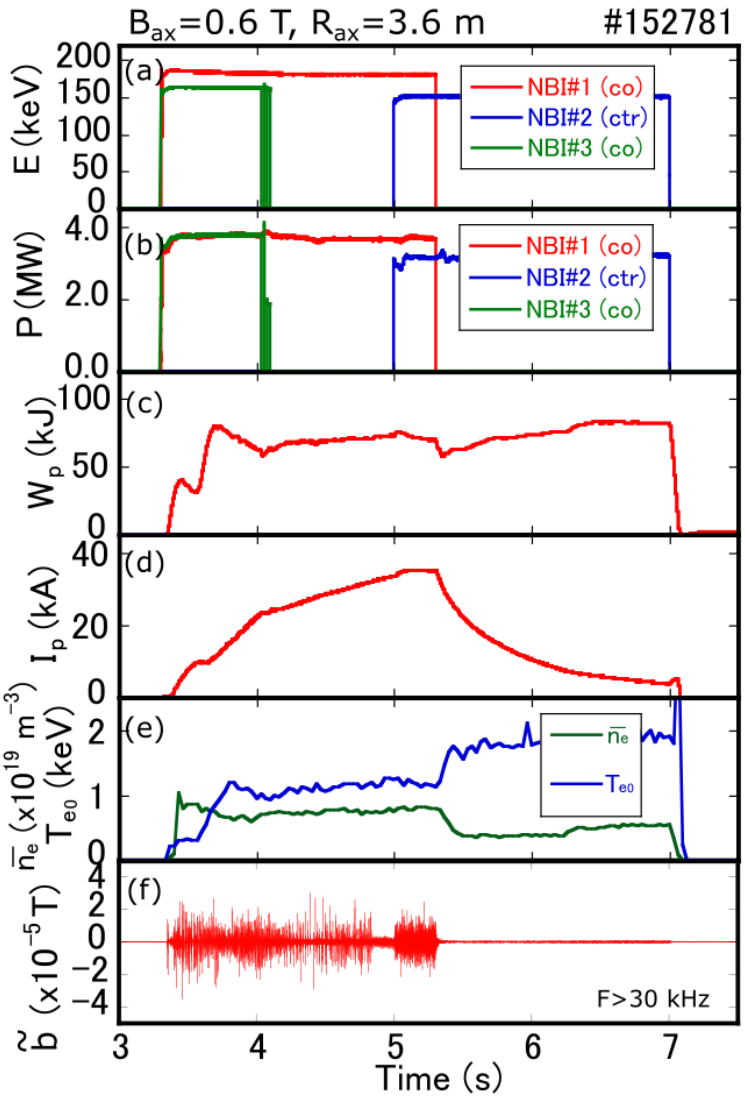

Figure 3. Time evolutions of the (a) injection energies and (b) injection powers of NBIs, (c) stored energy, (d) plasma current, (e) electron density n_e and temperature T_e, and (f) magnetic field measured by magnetic probe.

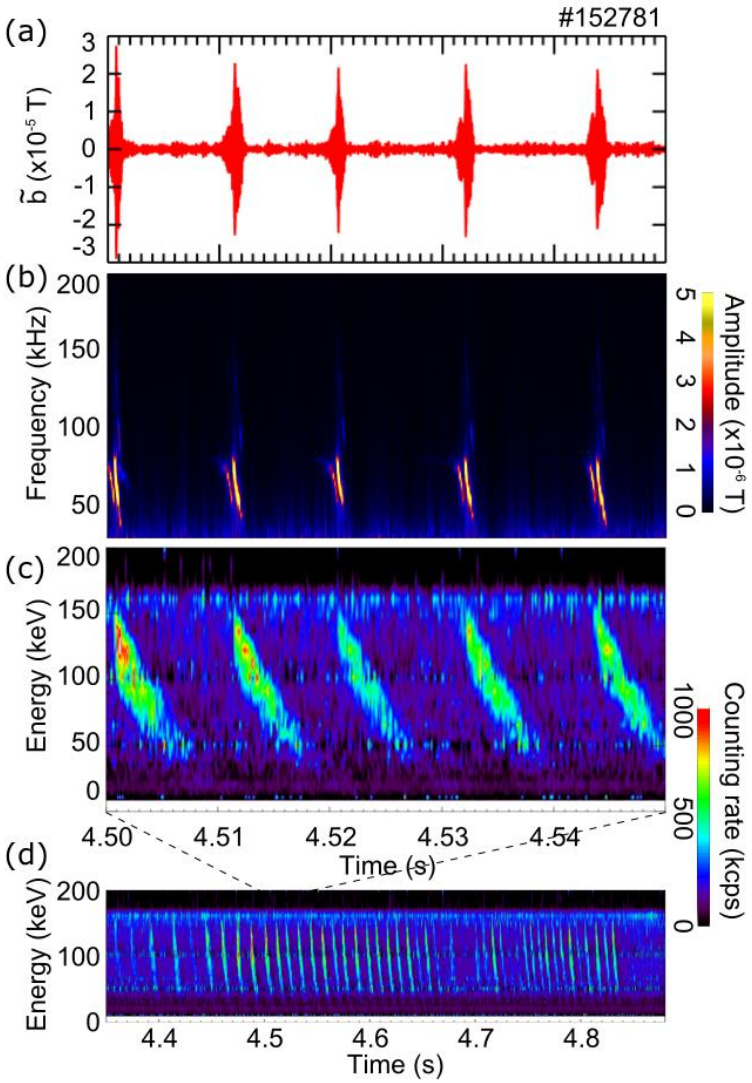

Figure 4. Time evolutions of the (a) signal of the Mirov coil, (b) the spectrogram of the magnetic fluctuations, and (c) the energy spectrum of the particle flux Γ observed by E||B-NPA. (d) The time evolution of the particle flux Γ with wider time range.

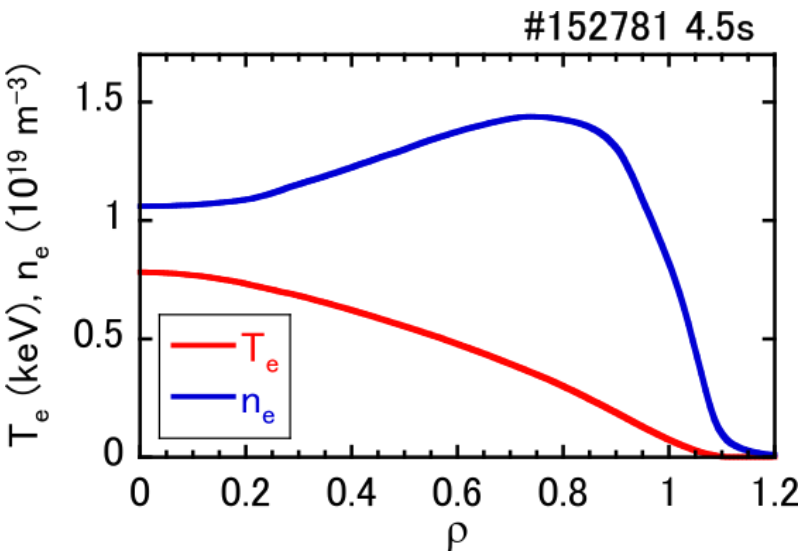

Figure 5. Distributions of T_e and the n_e measured by Thomson scattering.

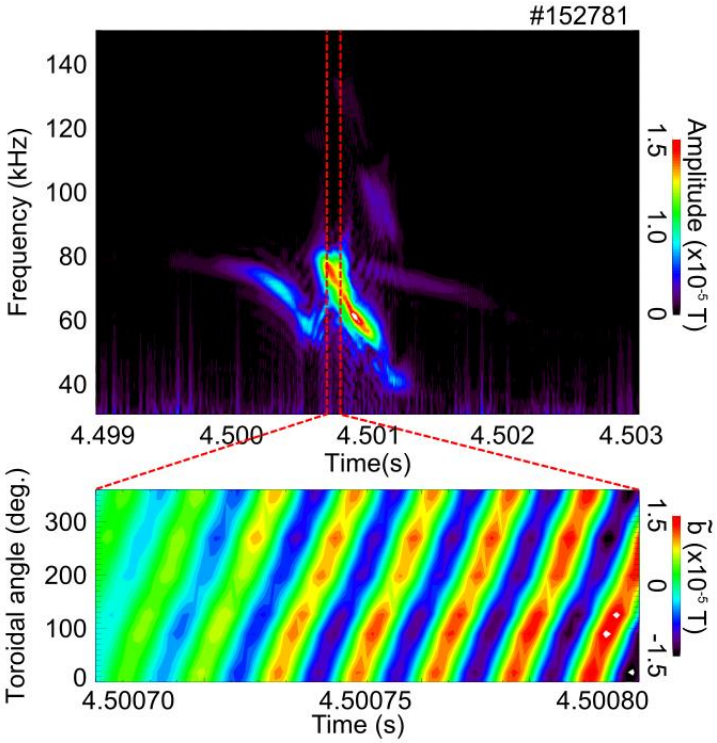

Figure 6. The spectrogram of the magnetic fluctuation during the TAE burst. The toroidal mode number clearly appeared with n=1.

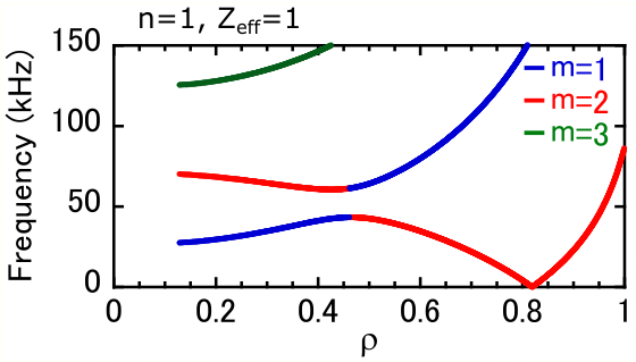

Figure 7. The calculated shear Alfvèn spectrum with *n*=1, the location of the mode coupling is considered to be around ρ=0.4-0.5, with *m*=1+2.

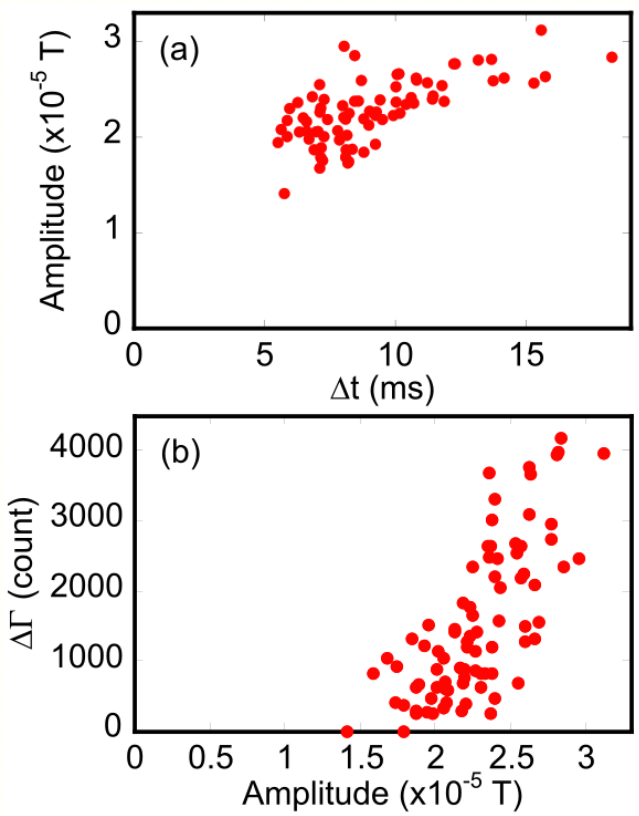

Figure 8. (a) Amplitude of the fluctuations with the interval of the burst to burst. (b) Amplitude of the fluctuations compared with the E||B-NPA ΔΓ.

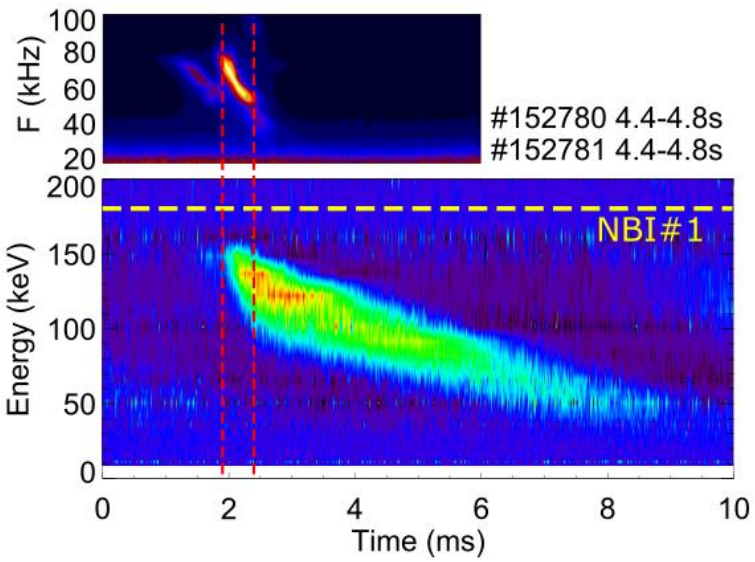

Figure 9. The conditional averaged spectrogram of the magnetic fluctuation and the $\Delta\Gamma$ observed by E||B-NPA. Red dashed lines are the timing of the start and the end of the TAE bursts. Yellow dashed line indicates the injection energy of the NBI #1.

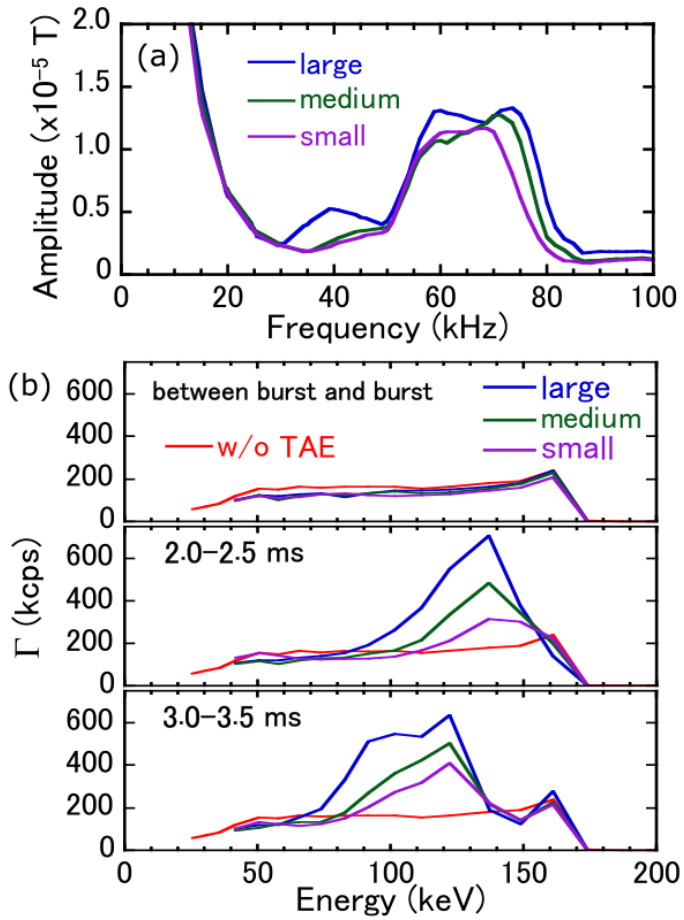

Figure 10. (a) The peak amplitude of the magnetic fluctuations of each frequency. The TAE bursts are divided into three groups by the amplitude of 75-80 kHz. (b) The Γ of without TAE burst, and three groups of each timing.

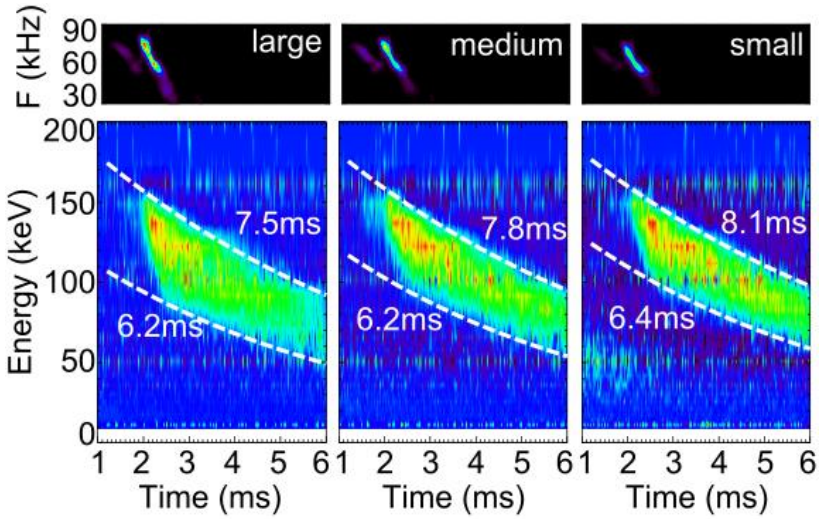

Figure 11. The time evolutions of the spectrogram of the magnetic fluctuations and $\Delta\Gamma$ measured by E||B-NPA, conditional averaging with divided into three groups. White dashed lines are the results of the energy slowing down time fitting at the edge.

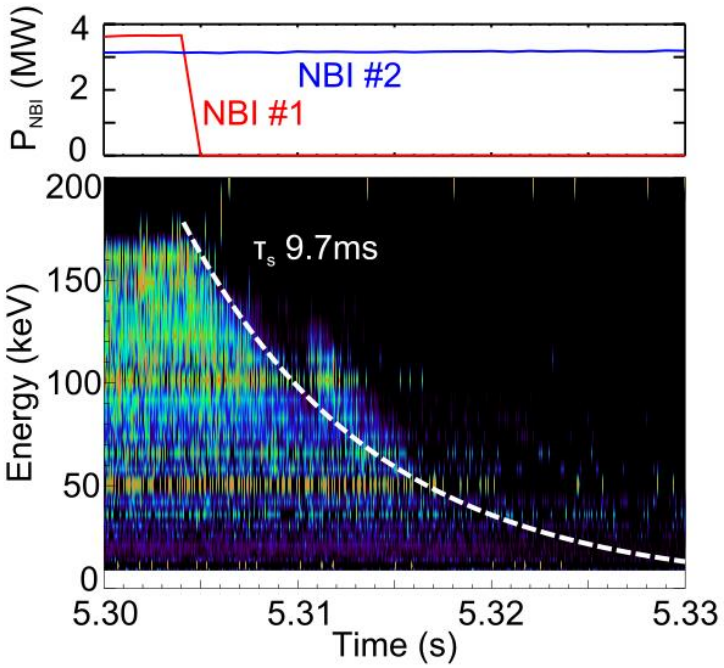

Figure 12. The time evolutions of injection powers of the NBIs and the counting rate of the E||B-NPA for estimating the slowing down estimation. By the fitting after the injection beam power turning off, the slowing down time is estimated to be 9.7 ms.

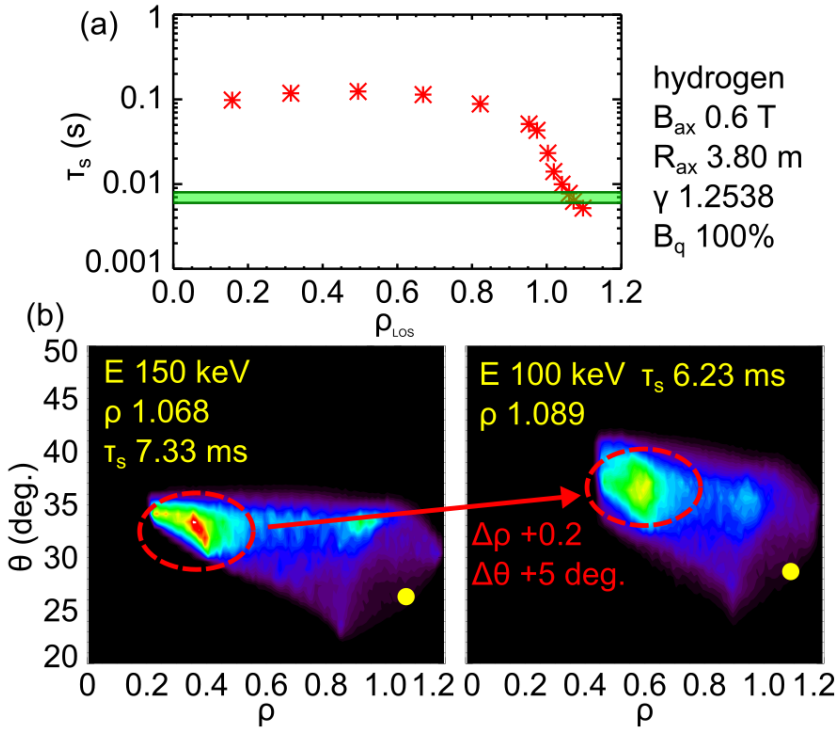

Figure 13. Results of the orbit trace code LORBIT. (a) The energy slowing down time τ_s of each trace started from various ρ_{LOS}. Green hatched τ_s is the energy slowing down time observed by E||B-NPA. (b) The ρ and the θ of the tracing particles. The color contours are the time duration while the particle pass through the ρ with the θ. The yellow circles indicate the charge exchanged locations. The red dashed circles indicate the location of the longest time duration.

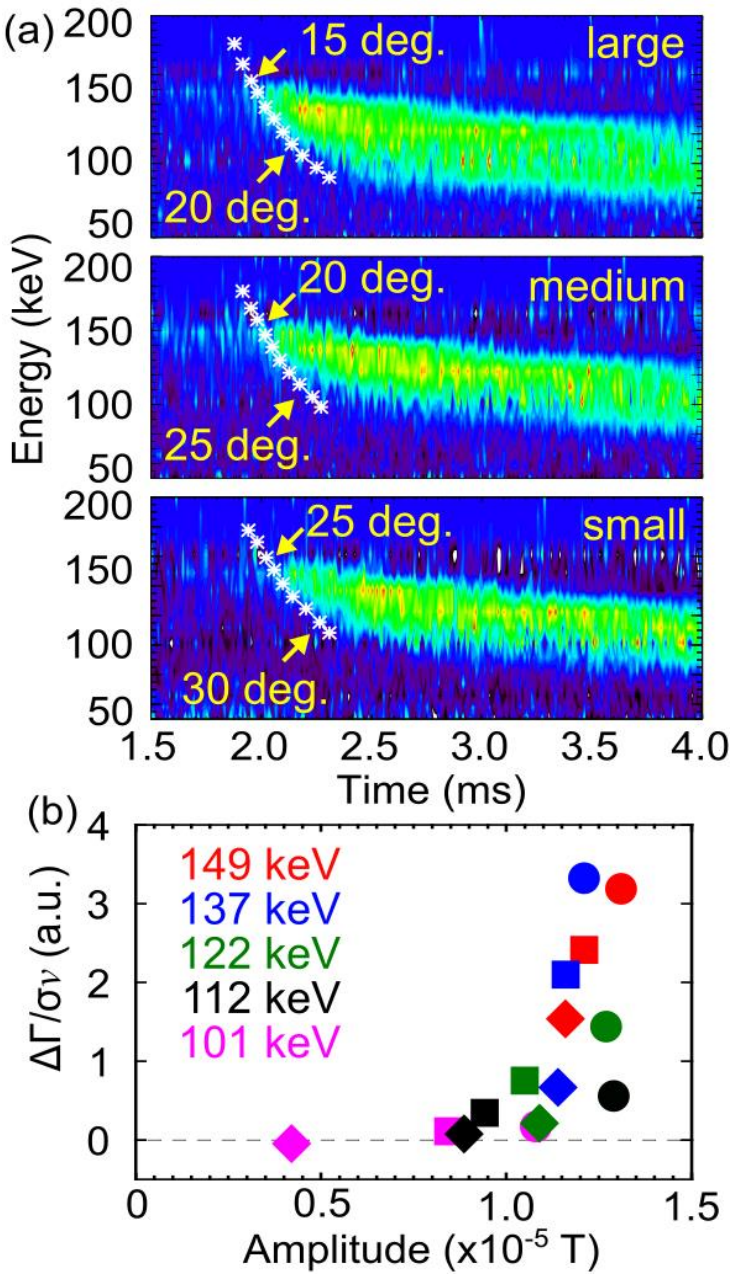

FIG. 14. (a) The conditional averaged ΔΓ with three groups (color contour), peak of the magnetic fluctuations with corresponding energy (white asterisk). (b) The amplitude of the magnetic fluctuation corresponding to each energy, and ΔΓ counts totaled 0.1 ms after the peak of the fluctuations. ΔΓ is divided by σv.